

A Mechanistic Model of the Intravitreal Pharmacokinetics of Large Molecules and the Pharmacodynamic Suppression of Ocular Vascular Endothelial Growth Factor Levels by Ranibizumab in Patients with Neovascular Age-Related Macular Degeneration

Laurence A. Hutton-Smith,^{*,†} Eamonn A. Gaffney,[†] Helen M. Byrne,[†] Philip K. Maini,[†] Dietmar Schwab,[‡] and Norman A. Mazer^{*,‡}

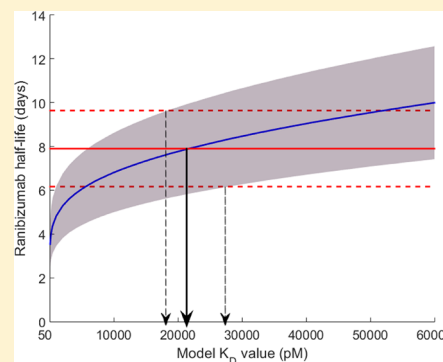
[†]Wolfson Centre For Mathematical Biology, Mathematical Institute, Andrew Wiles Building, University of Oxford, Radcliffe Observatory Quarter, Woodstock Road, Oxford OX2 6GG, U.K.

[‡]Clinical Pharmacology, Roche Pharma Research and Early Development, Roche Innovation Center Basel, Building 663/2130.12, Hochstrasse 16, 4070 Basel, Switzerland

S Supporting Information

ABSTRACT: Intravitreal injection of anti-VEGF (vascular endothelial growth factor) antibodies or antibody fragments has been shown to be a highly effective treatment for neovascular age-related macular degeneration (wet AMD). The ocular half-life ($t_{1/2}$) of these large molecules, determined in ocular fluids or derived from serum levels, varies with molecular size and is larger in humans than in preclinical animal species. The high affinity binding of VEGF to these molecules lowers the free concentration of VEGF and reduces its occupancy on VEGF receptors in ocular tissues. To understand the biophysical determinants of $t_{1/2}$ for anti-VEGF antibodies and the time-course of VEGF in ocular fluids, we developed a mechanistic model of intravitreal pharmacokinetics (IVT PK) for anti-VEGF antibodies and combined it with a mechanistic model of the pharmacodynamics (RVR PD) of VEGF suppression by ranibizumab, an anti-VEGF recombinant, humanized monoclonal antibody fragment (Fab). Our IVT PK model predicts that the ocular $t_{1/2}$ of a large molecule will be approximately four-times the calculated value of its vitreous diffusion time (T_{diff}), defined as $r_{vit}^2/6D$, where r_{vit} is the radius of the vitreous chamber in that species (modeled as a sphere), and D is the diffusion coefficient of the molecule in physiological saline at 37 °C obtained from the Stokes–Einstein relation. This prediction is verified from a compilation of data and calculations on various large molecules in the human, monkey, rabbit, and rat and is consistent with the reported $t_{1/2}$ values of ranibizumab in humans (mean value 7.9 days) and the calculated T_{diff} of 1.59 days. Our RVR PD model is based on the publication of Saunders et al. (*Br. J. Ophthalmol.* **2015**, *99*, 1554–1559) who reported data on the time-course of VEGF levels in aqueous humor samples obtained from 31 patients receiving ranibizumab treatment for wet AMD and developed a compartmental mathematical model to describe the VEGF suppression profiles. We modified Saunders' model with the known 2:1 stoichiometry of ranibizumab-VEGF binding and included the association and dissociation kinetics of the binding reactions. Using the RVR PD model, we reanalyzed Saunders' data to estimate the *in vivo* dissociation constant (K_D) between ranibizumab and VEGF. Our analysis demonstrates the delicate interrelationship between the *in vivo* K_D value and the intravitreal half-life and yields an *in vivo* K_D estimate that is appreciably larger than the *in vitro* K_D estimates reported in the literature. Potential explanations for the difference between the *in vivo* and *in vitro* K_D values, which appear to reflect the different methodologies and experimental conditions, are discussed. We conclude that the combined mechanistic model of IVT PK and RVR PD provides a useful framework for simulating the effects of dose, K_D , and the molecular weight of VEGF-binding molecules on the duration of VEGF suppression.

KEYWORDS: intravitreal, pharmacokinetics, VEGF, ranibizumab, neovascular age-related macular degeneration, mechanistic modeling



INTRODUCTION

Choroidal neovascular age-related macular degeneration or “wet AMD” is the leading cause of blindness in the elderly, cases of which are predicted to rise by 50% to 3 million in the United States alone by 2020.¹ The progression and severity of the pathogenesis of wet AMD are primarily mediated by

Special Issue: Ocular Therapeutics: Drug Delivery and Pharmacology

Received: November 10, 2015

Revised: December 18, 2015

Accepted: January 4, 2016

Published: January 4, 2016

vascular endothelial growth factors (principally VEGF-A²), which promote the development of highly permeable vasculature in the retina.³ Ranibizumab (Lucentis, Genentech Inc., San Francisco, CA), an anti-VEGF recombinant, humanized monoclonal antibody fragment (Fab), is administered by intravitreal (IVT) injection and has been shown to be highly effective in the treatment of wet AMD, halting and even reversing its development.⁴ Ranibizumab binds with high affinity to VEGF, a homodimeric molecule, neutralizing it as a pro-angiogenic factor by blocking its interaction with VEGF receptors, found on the surface of the vascular endothelial cells in the retina.

The IVT pharmacokinetics (PK) of ranibizumab and other large molecules that bind VEGF has been studied previously in humans and preclinical animal species by direct analysis of drug levels in the aqueous or vitreous humor or by indirect modeling of serum drug levels.^{5–14} In a given species, the ocular half-life ($t_{1/2}$) is found to increase modestly with the molecular weight of the compound; comparisons of the same molecule across species show that the $t_{1/2}$ values generally become larger as the size of the eye increases. For ranibizumab, the $t_{1/2}$ value in humans has been estimated to be 7.9 days (mean value of two studies; Krohne¹¹ and Xu¹²) compared to 3.3 and 3.1 days in the monkey^{7,8} and rabbit,^{9,13} respectively.

In a series of elegant clinical studies, Fauser's group measured free VEGF levels in aqueous humor samples obtained from patients with wet AMD before and after IVT injections with ranibizumab.^{15–17} Recently, the data from 31 patients were published, and the time-course of the free VEGF levels was modeled by Saunders et al.¹⁷ In this model, the K_D value for ranibizumab binding to VEGF was assumed to be 46 pM, based on an *in vitro* binding study¹⁸ at 25 °C, and the $t_{1/2}$ for ranibizumab as well as for VEGF and the VEGF-ranibizumab (VR) complex was estimated from the model to be 3.5 days, roughly two-fold smaller than the experimentally determined $t_{1/2}$ for ranibizumab in humans.

To quantitatively understand the biophysical determinants of the IVT $t_{1/2}$ of large molecules and the time-course of VEGF suppression after ranibizumab injection, we have developed a mechanistic model of the pharmacokinetics of IVT administration and the pharmacodynamics of VEGF suppression by ranibizumab.

Our model of IVT PK is based in part on Missel's simulations of IVT injection in the rabbit, monkey, and human,¹⁹ which describes the role of intravitreal diffusion and convection, and the interfacial area between the vitreous and aqueous humor through which large molecules must pass to be eliminated from the eye. Our RVR PD model is built on Saunders' model but uses the known stoichiometry (2:1) for the binding of ranibizumab to the VEGF homodimer and therefore includes a description of the VEGF-ranibizumab (VR) and ranibizumab-VEGF-ranibizumab (RVR) complexes. In addition, we treat binding as a dynamic process rather than assuming quasi-equilibrium. Lastly, in view of the inconsistencies among *in vitro* K_D values for VEGF-ranibizumab binding^{18,20} and the lack of an established *in vivo* K_D value in the vitreous humor, we have treated K_D as a parameter in our model and explored the interrelationship between the *in vivo* K_D value and the ranibizumab $t_{1/2}$ in a reanalysis of Saunders' data.

We believe that our mechanistic model offers a self-consistent interpretation of the available PK and PD data for ranibizumab and other large molecules and provides a useful

framework for simulating the effects of dose, K_D , and molecular weight for the design of future large molecules that suppress VEGF.

METHODS

Mechanistic Model of IVT PK. Following Missel,¹⁹ we assume that the principal pathway for the ocular clearance of large molecules is by a first-order transfer process from the vitreous to the aqueous chambers, from which the molecule is absorbed into the circulation via Schlemm's canal by the physiological process of aqueous humor turnover. To model the elimination rate constant (k_{el}) from the vitreous into the aqueous chamber, we approximate the vitreous chamber as a sphere with radius r_{vit} as shown in Figure 1. Denoting the total

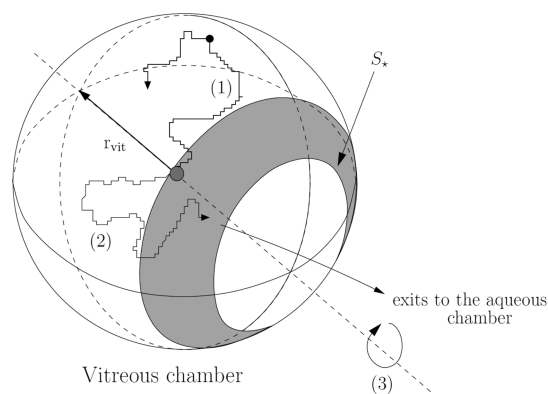


Figure 1. Spherical approximation for the vitreous chamber with radius r_{vit} . S^* is the area of the interface through which the vitreous chamber communicates with the aqueous (anterior) chamber. Path 1 shows the random walk of a molecule, originating at the center, that does not reach the interface. Path 2 shows the random walk of a molecule that reaches S^* and exits to the aqueous chamber. The dashed line passing from the posterior to the anterior of the vitreous chamber (3) is the axis of spherical symmetry.

surface area by S , we define the portion of the surface area through which a molecule can transfer to the aqueous chamber as S^* . By making the well-mixed assumption, the average location of any molecule within the vitreous chamber is at its center, and therefore the average vitreous diffusion time (T_{diff}) for any particle to reach the surface of the sphere can be estimated using the Brownian motion description of the mean square displacement of a particle in three dimensions (eq 1):

$$T_{diff} = \frac{r_{vit}^2}{6D} \quad (1)$$

where the diffusion coefficient, D , can be calculated using the Stokes–Einstein relation (eq 2) where k_B and T are the Boltzmann constant and absolute temperature, η corresponds to the viscosity of physiological saline (0.15 M NaCl) at 37 °C, and the hydrodynamic radius R_h is estimated from the molecular weight (MW), Avogadro's number (N_A), and the partial specific volume of protein (v), taken as 0.73 cm³/g,²¹ assuming an equivalent sphere (eq 3):

$$D = \frac{k_B T}{6\pi\eta R_h} \quad (2)$$

$$R_h = \left(\frac{3\nu MW}{4\pi N_A} \right)^{1/3} \quad (3)$$

The resulting values of D are proportional to $MW^{-1/3}$ (Table 1).

Table 1. Molecular Properties of Antibodies Analyzed. Molecular Weight (MW), Hydrodynamic Radius (R_h), and Diffusion Coefficient (D) at 37 °C in Physiological Saline for Ranibizumab (R), Bevacizumab, a Fab-Dimer, VEGF (V), the VEGF-Ranibizumab Complex (VR), and the Ranibizumab-VEGF-Ranibizumab Complex (RVR)

molecule	MW (kDa)	R_h (nm)	D (cm ² /sec)
ranibizumab (R), Fab	48.35 ⁴	2.4	1.34×10^{-6}
bevacizumab, IgG	150 ^{13,24}	3.51	9.13×10^{-7}
Fab-dimer	100 ¹³	3.07	1.05×10^{-6}
VEGF (V)	40 ³	2.26	1.42×10^{-6}
VR	88.35	2.95	1.09×10^{-6}
RVR	136.7	3.41	9.42×10^{-7}

Postulating the diffusion (Brownian movement) from the vitreous to the aqueous chamber to be the primary mechanism for large molecule elimination from the eye, we propose the following expression for kel:

$$kel = \frac{S^*}{S} \frac{1}{T_{diff}} \quad (4)$$

This expression is based on the following assumptions. First, the hyaloid membrane separating the vitreous and aqueous chamber is highly porous²² so that a molecule immediately leaves the vitreous chamber upon contact with S^* . Second, there is no back diffusion from the aqueous chamber due to the high flow rate of the aqueous humor.¹⁹ Finally, kel will be the product of the probability per unit time that a molecule diffuses from the center of the vitreous chamber (modeled as a sphere) to the perimeter ($1/T_{diff}$) and the probability of a particle encountering the hyaloid membrane, given by S^*/S . As discussed later, this result is an approximation for the solution of the “first-passage problem”²³ evaluated at the center of the spherical geometry depicted in Figure 1.

By definition, the elimination rate of a molecule, kel, is related to its half-life, $t_{1/2}$, via the expression:

$$kel = \frac{\log 2}{t_{1/2}} \quad (5)$$

By substituting eq 5 into eq 4, we obtain the following relationship between $t_{1/2}$ and T_{diff} :

$$t_{1/2} = \log 2 / \left(\frac{S^*}{S} \right) T_{diff} \quad (6)$$

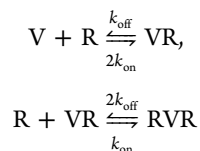
Using the anatomical data given in Missel’s paper, we estimate the ratio S^*/S to be 0.23 for the rabbit, 0.13 for the monkey, and 0.15 for the human, which correspond to a mean value of 0.17 (see Supporting Information; section S1). The similarity of these ratios suggests a general anatomical relationship across species so that eq 6 implies that $t_{1/2}$ will be approximately four-times the calculated value of T_{diff} for all large molecules and across all species based on the mean value of S^*/S .

Since $D \propto MW^{-1/3}$ (eqs 2 and 3), we may then derive the following scaling relationship between molecular species i and j :

$$kel_i = \left(\frac{MW_j}{MW_i} \right)^{1/3} kel_j \quad (7)$$

Given the vitreal $t_{1/2}$ of ranibizumab, we can use eqs 5 and 7 to estimate kel values for other molecules of interest (as discussed in the next section).

Pharmacodynamic Model of VEGF Suppression by Ranibizumab—The RVR Model. Following Saunders,¹⁷ our mathematical description of VEGF suppression was formulated using the two-compartment representation shown in Figure 2. We considered only the vitreous and aqueous chambers of the eye, as the former is the site of ranibizumab injection, and the latter is where the experimental VEGF samples were collected. VEGF (V), a homodimer, has two identical binding sites for ranibizumab.²⁵ Therefore, according to the notation in Table 2, we defined the following sequential reaction scheme:



Notice that in the first reaction there are two equivalent sites of association, while in the second reaction there are two equivalent sites of dissociation. As a consequence, the equilibrium dissociation constant for the first reaction corresponds to $K_D/2$ and for the second reaction is $2K_D$, where $K_D = k_{off}/k_{on}$ is the hypothetical value for a single VEGF-ranibizumab binding site.

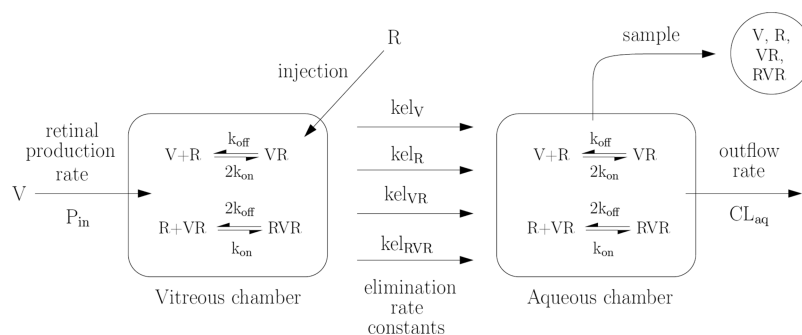


Figure 2. Two-compartment PD model of VEGF (V) and ranibizumab (R) interaction in the eye is composed of the vitreous and aqueous chambers. Note the arrow labeled “sample” indicates that the experimental samples were collected from the aqueous humor.

Table 2. Chemical Species and Notation Used in the Model. All Concentrations Are Functions of Time (t) with Units of pM. Subscripts Denote the Concentrations of Each Variable in the Vitreous and Aqueous Chambers

chemical species	chemical notation	concentration (pM)
VEGF free (unbound)	V	vitreous v_{vit}
		aqueous v_{aq}
ranibizumab free (unbound)	R	vitreous r_{vit}
		aqueous r_{aq}
VEGF ranibizumab complex	VR	vitreous vr_{vit}
		aqueous vr_{aq}
VEGF ranibizumab dimer complex	RVR	vitreous rvr_{vit}
		aqueous rvr_{aq}

In patients with wet AMD, VEGF production in the retina and its subsequent diffusion into the vitreous chamber are described in our model as production of V at the rate P_{in} (see the leftmost arrow in Figure 2). Ranibizumab is delivered to patients via intravitreal injection, which we capture in the initial condition for $r_{vit}(t)$. Unlike the Saunders model, we allow association and dissociation kinetics to occur in both the vitreous and aqueous chambers. As discussed in the previous section (IVT PK model), we assume that the major pathway of ocular elimination for the four species is via the unidirectional transfer from the vitreous to the aqueous chambers, represented by the elimination rate constants kel_R , kel_V , kel_{VR} , and kel_{RVR} , which depend on the MW of each species (see Table 1). Here, we have assumed no backward transport from the aqueous to the vitreous chambers and neglect the possible elimination of these molecules via the retina.

Since T_{diff} is smaller than $1/kel$ by the factor S^*/S (eq 4), we assume the system to be well-mixed, allowing for the construction of a system of coupled nonlinear, time-dependent ordinary differential equations (ODEs). Chemical reactions are described using the law of mass action, giving the following equations for the time-evolutions of the chemical concentrations.

VITREOUS CHAMBER

$$\frac{dv_{vit}}{dt} = (k_{off}vr_{vit} - 2k_{on}v_{vit}r_{vit}) - kel_Vv_{vit} + \frac{P_{in}}{Vol_{vit}} \quad (8)$$

$$\begin{aligned} \frac{dr_{vit}}{dt} &= (k_{off}vr_{vit} - 2k_{on}v_{vit}r_{vit}) + (2k_{off}rvr_{vit} - k_{on}r_{vit}vr_{vit}) \\ &\quad - kel_Rr_{vit} \end{aligned} \quad (9)$$

$$\begin{aligned} \frac{dvr_{vit}}{dt} &= -(k_{off}vr_{vit} - 2k_{on}v_{vit}r_{vit}) + (2k_{off}rvr_{vit} - k_{on}r_{vit}vr_{vit}) \\ &\quad - kel_{VR}vr_{vit} \end{aligned} \quad (10)$$

$$\frac{drvr_{vit}}{dt} = -(2k_{off}rvr_{vit} - k_{on}r_{vit}vr_{vit}) - kel_{RVR}rvr_{vit} \quad (11)$$

AQUEOUS CHAMBER

$$\frac{dv_{aq}}{dt} = (k_{off}vr_{aq} - 2k_{on}v_{aq}r_{aq}) + \left(\frac{Vol_{vit}}{Vol_{aq}}\right)kel_Vv_{vit} - \frac{CL_{aq}}{Vol_{aq}}v_{aq} \quad (12)$$

$$\begin{aligned} \frac{dr_{aq}}{dt} &= (k_{off}vr_{aq} - 2k_{on}v_{aq}r_{aq}) + (2k_{off}rvr_{aq} - k_{on}r_{aq}vr_{aq}) \\ &\quad + \left(\frac{Vol_{vit}}{Vol_{aq}}\right)kel_Rr_{vit} - \frac{CL_{aq}}{Vol_{aq}}r_{aq} \end{aligned} \quad (13)$$

$$\begin{aligned} \frac{dvr_{aq}}{dt} &= -(k_{off}vr_{aq} - 2k_{on}v_{aq}r_{aq}) + (2k_{off}rvr_{aq} - k_{on}r_{aq}vr_{aq}) \\ &\quad + \left(\frac{Vol_{vit}}{Vol_{aq}}\right)kel_{VR}vr_{vit} - \frac{CL_{aq}}{Vol_{aq}}vr_{aq} \end{aligned} \quad (14)$$

$$\begin{aligned} \frac{drvr_{aq}}{dt} &= -(2k_{off}rvr_{aq} - k_{on}r_{aq}vr_{aq}) + \left(\frac{Vol_{vit}}{Vol_{aq}}\right)kel_{RVR}rvr_{vit} \\ &\quad - \frac{CL_{aq}}{Vol_{aq}}rvr_{aq} \end{aligned} \quad (15)$$

where Vol_{vit} and Vol_{aq} denote the volumes of the vitreous and aqueous chambers (mL), respectively, and CL_{aq} represents the clearance rate from the aqueous chamber (mL/day), taken to be equal to the production rate of aqueous humor. We assume the initial VEGF levels to be at the drug-free equilibrium levels predicted by this model and all complexes to be absent. To simulate a single intravitreal dose, the initial vitreous concentration (pM) for ranibizumab is set equal to $d_0/MW_R/Vol_{vit} \times 10^{12}$ where d_0 is the ranibizumab dosage (0.5 mg) injected into the vitreous chamber. The initial ranibizumab concentration in the aqueous chamber is set to zero.

Clinical Data. We utilized the recently published data by Saunders¹⁷ wherein 31 patients with wet AMD were studied following the administration of intravitreal 0.5 mg doses of ranibizumab after various time intervals. Patients were submitted to aqueous humor sampling prior to the time of dosing and at later dates over several months. Free VEGF concentrations were measured from the aqueous humor samples using Luminex multiplex bead analysis (Luminex, Austin, Texas, USA). Zhu²⁶ has demonstrated that this assay measures free (unbound) VEGF levels in the presence of the anti-VEGF antibody bevacizumab. Graphical data reported in the supplementary file by Saunders were digitized for all 31 subjects using Plot Digitizer Version 2.0 (Dept. of Physics, University of South Alabama).

Methods of Parameter Estimation and Optimization. The parameters used in the model, and their values, are stated in Table 3. We derived estimates of $t_{1/2R}$ and P_{in} for each patient as a function of K_D by fitting the patient-specific data over a range of K_D values (50 to 60 000 pM); an optimization procedure was used for a given value of K_D with respect to $t_{1/2R}$ and P_{in} . This was achieved using `fmincon`²⁷ (part of MATLAB's global optimization toolbox), which for a given function seeks a local minimum in parameter space by following a local negative gradient. For our purposes, we sought to minimize the root-mean-square error (RMSE) of the solution (solved using MATLAB's stiff ODE solver `ode23s`) with respect to individual patient data. To locate the global minimum in this process, multiple initial estimates of $t_{1/2R}$ were taken between 2 and 15 days. An accurate initial estimate for P_{in} was derived from the average of the initial and final VEGF data points.

Table 3. Summary of Parameter Values and Notation Used within the Model. Parameters with Stated Numerical Values Were Fixed as Constants for All Patients. k_{on} Is Expressed in Terms of the Dissociation Constant $K_D = k_{off}/k_{on}$. Value of K_D Was Treated as an Input to the Model and Varied over the Range 50 to 60 000 pM. Values of P_{in} and $t_{1/2R}$ Are Patient Specific and Were Estimated for Each Patient as a Function of the Input Value of K_D . Estimates of the Rate Constants kel_R , kel_V , kel_{VR} , and kel_{RVR} Were Derived from $t_{1/2R}$ Using Eqs 5 and 7

parameter	value	units	description
k_{off}	0.864 ²⁰	day ⁻¹	reaction rate of VR → V + R
k_{on}	k_{off}/K_D	day ⁻¹ pM ⁻¹	reaction rate of R + VR → RVR
K_D	input	pM	dissociation constant
CL_{aq}	3.6 ²⁸	mL day ⁻¹	aqueous humor clearance rate
P_{in}	estimated	fmol day ⁻¹	VEGF production rate
Vol_{vit}	4.5 ^{6,26}	mL	volume of the vitreous
Vol_{aq}	0.16 ^{29,30}	mL	volume of the aqueous
d_0	0.5 ¹⁵	mg	initial dose of ranibizumab
$t_{1/2R}$	estimated	days	ranibizumab vitreal half-life
kel_R	derived	day ⁻¹	vitreal elimination rate constant for R
kel_V	derived	day ⁻¹	vitreal elimination rate constant for V
kel_{VR}	derived	day ⁻¹	vitreal elimination rate constant for VR
kel_{RVR}	derived	day ⁻¹	vitreal elimination rate constant for RVR

RESULTS

Relationship between Ocular Half-Life and Vitreous Diffusion Time. On the basis of eq 6, we predict that the ocular half-life of a large molecule ($t_{1/2}$) should be proportional to its vitreous diffusion time (T_{diff}) with a proportionality factor of approximately 4. To test this prediction, we performed a meta-analysis of experimental $t_{1/2}$ data across animal species and molecules by computing the T_{diff} values corresponding to those molecules and species using eq 1. Table 4 provides a compilation of $t_{1/2}$ data taken from the literature for ranibizumab, Fab fragments, bevacizumab, IgG antibodies, and Fab-dimer fragments in the human, monkey, rabbit, and rat. Estimates of the vitreous volume (Vol_{vit}) and radius of the equivalent vitreous sphere (r_{vit}) are provided for each species along with the calculated T_{diff} values.

By plotting the individual $t_{1/2}$ data in Figure 3 versus the calculated T_{diff} values, we observe the proportionality predicted by eq 6. Linear regression through the origin gives a slope of 4.4 (95% confidence interval 4.1–4.7), in close agreement with

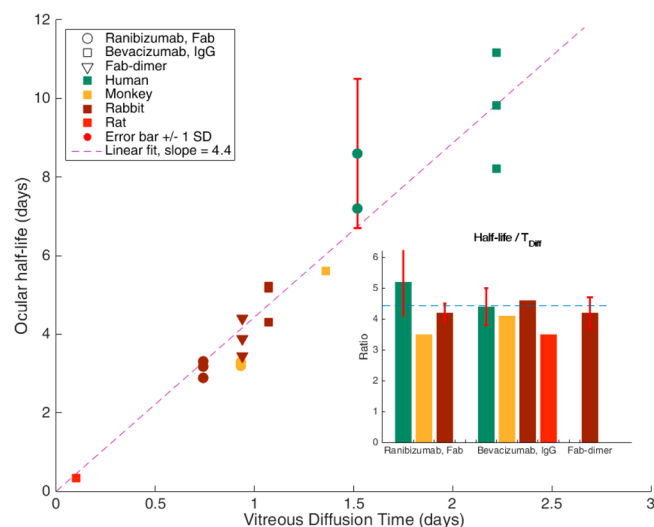


Figure 3. Ocular half-life data from individual studies plotted against vitreous diffusion times for various molecules and animal species using data from Table 4. Linear regression through the origin yields a line with slope 4.4 (95% confidence interval 4.1–4.7), in close agreement with the predicted value based on eq 6. The insert depicts the mean ratios $t_{1/2}/T_{diff}$; the dashed horizontal line equals 4.4.

the predicted value of 4 that was derived from the mean value of S^*/S (see Methods).

This meta-analysis provides strong evidence that the experimentally determined ocular $t_{1/2}$ of ranibizumab in humans of approximately 7.9 days (mean of two independent studies) is consistent with the overall relationship predicted by eq 6.

Reanalysis of Saunders' VEGF Data Using the RVR PD Model. Figure 4 shows the optimized fits of the RVR PD model to the data of a typical patient (#40) for different input values of K_D . As K_D increases from 50 to 60 000 pM, the fitted curves change shape, and the estimated values of $t_{1/2R}$ increase from 3.3 days to 9.8 days. The corresponding RMSE values of the fit change only slightly as K_D varies (see caption of Figure 4).

By varying K_D over the same range for all 31 subjects, we show in Figure 5 how the mean \pm SD of the estimated values of $t_{1/2R}$ depends on K_D (blue curve and shaded gray region). The relationship between K_D and $t_{1/2R}$ seen for patient #40 is observed for all patients. Over this range of K_D values, the variation of RMSE for each patient was generally quite small (see Figure S4.1 in the Supporting Information). Individual patient fits, parameters, and RMSE values can be found in

Table 4. Literature Compilation of Ocular Half-Lives and Calculated Vitreous Diffusion Times for Different Animal Species and Large Molecules. Half-Lives Correspond to Mean (SD) of the Values from the Individual Studies Referenced. Vitreous Diffusion Times Were Calculated from Eq 1 Using the D Values of Table 1 and the r_{vit} Value for Each Species. Values in Parentheses Denote SDs where Available; r_{vit} Values Were Obtained by Approximating the Vitreous Chamber as a Sphere

species	ranibizumab, Fab					bevacizumab, IGg				Fab-dimer		
	name	Vol_{vit} (mL)	r_{vit} (cm)	$t_{1/2}$ (days)	T_{diff} (days)	$t_{1/2}/T_{diff}$	$t_{1/2}$ (days)	T_{diff} (days)	$t_{1/2}/T_{diff}$	$t_{1/2}$ (days)	T_{diff} (days)	$t_{1/2}/T_{diff}$
human (76 kg)		4.5 ^{6,26}	1.02	7.9 (1.74) ^{11,12}	1.52	5.2 (1.1)	9.73 (1.48) ^{5,6,24}	2.22	4.4 (0.7)	n/a ^b	n/a ^b	n/a ^b
monkey (2.2–4.5 kg)		2.17 ¹⁹	0.8	3.25 (0.06) ^{7,8}	0.93	3.5 (0.1)	5.6 ⁷	1.36	4.1	n/a ^b	n/a ^b	n/a ^b
rabbit (2.5–3 kg)		1.52 ¹⁹	0.71	3.12 (0.21) ^{9,13}	0.74	4.2 (0.3)	4.9 (0.04) ^{10,13}	1.07	4.6 (0.03)	3.91 (0.48) ¹³	0.94	4.2 (0.5)
rat (0.25–0.35 kg)		0.042 ³¹	0.22	n/a ^b	n/a ^b	n/a ^b	0.341 ^{14,a}	0.1	3.5	n/a ^b	n/a ^b	n/a ^b

^aSee Supporting Information (section S2) for estimation of $t_{1/2}$ and T_{diff} for bevacizumab in the rat. ^bn/a, not available.

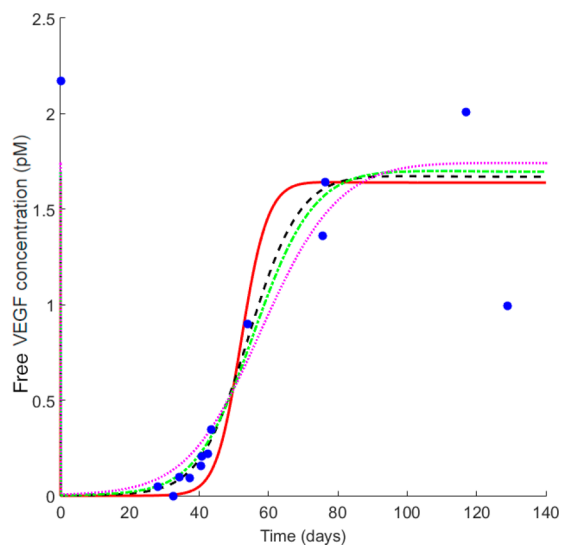


Figure 4. Series of optimized fits of the RVR model to the data of patient #40 (blue dots) as K_D varies. Key: $K_D = 50$ pM (red solid line, $t_{1/2} = 3.3$ days, RMSE = 0.27 pM), $K_D = 10\,000$ pM (black dashed line, $t_{1/2} = 6.4$ days, RMSE = 0.25 pM), $K_D = 21\,000$ pM (green dot/dash line, $t_{1/2} = 7.6$ days, RMSE = 0.25 pM), $K_D = 60\,000$ pM (purple dotted line, $t_{1/2} = 9.8$ days, RMSE = 0.26 pM).

section S3 of the [Supporting Information](#). We conclude that the VEGF data alone are insufficient to uniquely determine the *in vivo* value of K_D and the corresponding distribution of $t_{1/2R}$ values.

To estimate the *in vivo* value of K_D in [Figure 5](#), we overlay the experimentally determined values of the mean \pm SD of $t_{1/2R}$ (as indicated by the red line, with SD bounds indicated by dashed lines). From the region of intersection of the experimental range of $t_{1/2R}$ with the shaded area, we estimate

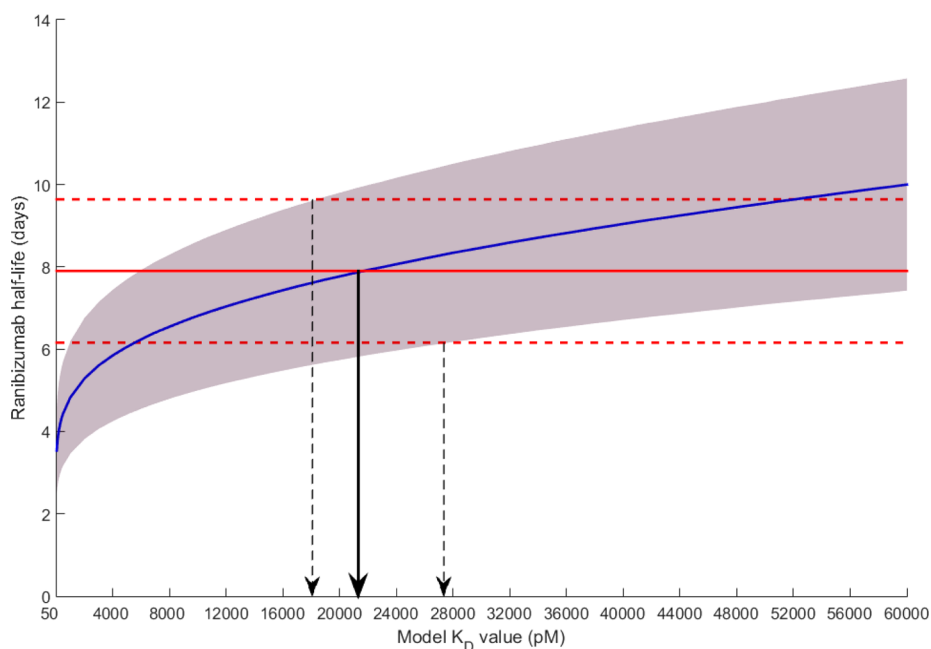


Figure 5. Mean (\pm SD) of model estimated $t_{1/2R}$ values (blue curve \pm SD in gray area) with respect to a K_D range of 50 to 60 000 pM. The solid red line shows the mean experimental ranibizumab $t_{1/2R}$ of 7.9 days in humans, and the dashed red lines indicate \pm SD (1.74 days). From the points of intersection of the solid and dashed red lines with the blue curve and gray area, we have estimated the *in vivo* value (range) of K_D as indicated by the vertical arrows pointing to the x-axis.

the *in vivo* value of K_D to lie in the range 18 084–27 361 pM, with an average value of 21 326 pM (21.3 nM).

Impact of Binding Stoichiometry and Kinetics and on the VEGF Profiles. Here, we demonstrate the effect of using the observed 2:1 stoichiometry of ranibizumab binding to VEGF and explore the influence of varying the parameter k_{off} on the VEGF profile.

[Figure 6](#), panel a shows the VEGF data from patient #40 with two model curves. The solid red line depicts the RVR model fit to the data for a K_D value of 21 000 pM, whereas the black dashed line shows the resulting curve if binding is restricted to only the VR binding model and optimized to fit the data. The RVR binding model provides a more accurate representation of the data with a $t_{1/2R}$ value of 7.6 days in contrast to the VR binding model with a $t_{1/2R}$ value of 9.3 days.

[Figure 6](#), panel b shows the effect on the VEGF profile of varying the dissociation rate constant k_{off} from its default value of 0.864 day^{-1} while holding K_D fixed at 21 000 pM. A 100-fold increase in k_{off} (black dashed curve) shifts the VEGF profile to the left of the red curve, while its shape is retained. The left-shift results from a rapid redistribution of previously bound R from the VR and RVR species brought on by the rapid dilution of all species in the aqueous humor. With a 100-fold decrease in k_{off} (green curve), the VEGF profile shifts further to the left but has a different shape from the other curves. It can be shown that the altered shape at low k_{off} values results from the very slow rates of association and dissociation between the R, V, VR, and RVR species, which are too slow to achieve the previously attained quasi-equilibrium states in the vitreous humor (see [Supporting Information](#), section S5 for the corresponding vitreous profiles). On the basis of this analysis, we conclude that for the default value of k_{off} , the VEGF profile in the vitreous humor is close to the quasi-equilibrium state, while the profile in the aqueous humor reflects a simple dilution of the vitreous profile, as the residence time in the aqueous humor

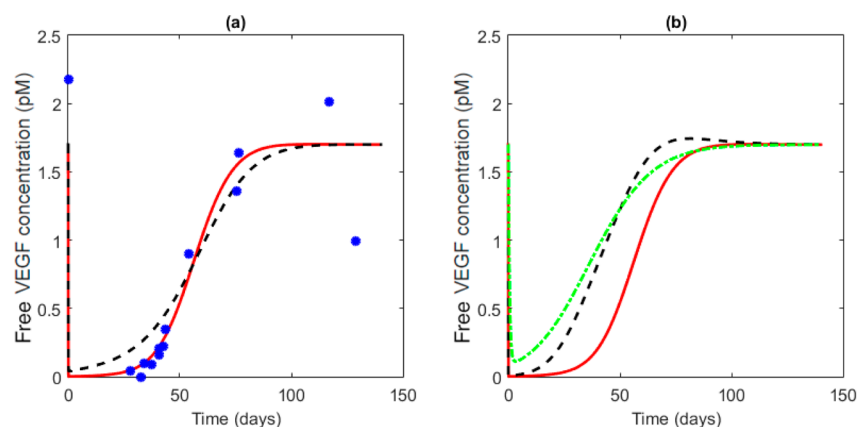


Figure 6. Aqueous compartment free VEGF suppression profiles, (a) effect of binding, RVR binding (solid red), VR binding (dashed black), (b) effect of dissociation rate constant, k_{off} : 0.864 day^{-1} (solid red, same as in panel a.), 86.4 day^{-1} (dashed black), 0.00864 day^{-1} (dot/dash green).

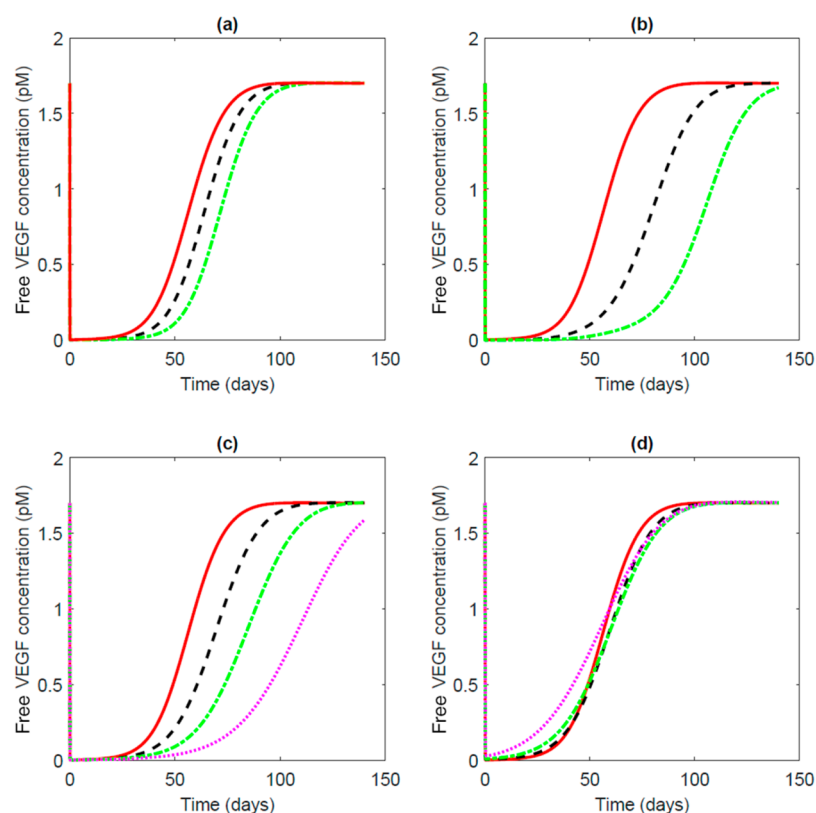


Figure 7. Aqueous compartment free VEGF suppression profiles: (a) simulated effect of increasing dose 0.5 mg (solid red), 1 mg (dashed black), 2 mg (dot/dash green); (b) simulated effect of lowering K_D with a constant half-life (7.6 days), 21 000 pM (solid red), 2100 pM (dashed black), 210 pM (dot/dash green); (c) simulated effect of increasing MW while adjusting the dose in proportion to MW : 48.35 kDa (solid red, dose 0.5 mg), 100 kDa (dashed black, 1 mg), 200 kDa (dot/dash green, 2 mg), 500 kDa (dotted purple, 5 mg); (d) simulated effect of increasing MW while keeping dosage constant at 0.5 mg: 48.35 kDa (solid red, $2.3 \times 10^6 \text{ pM}$), 100 kDa (dashed black, $1.1 \times 10^6 \text{ pM}$), 200 kDa (dot/dash green, $5.6 \times 10^5 \text{ pM}$), 500 kDa (dotted purple, $2.2 \times 10^5 \text{ pM}$).

(ca. 0.04 days; $\sim 1 \text{ h}$) is too short for redistribution of the bound R. This supports the assumption made by Saunders¹⁷ and shows the subtle influence of the k_{off} values on the behavior of the PK/PD model.

Impact of Dose, K_D , and MW on VEGF Profiles. Using the estimated *in vivo* K_D value of 21 000 pM, we demonstrate in Figure 7, panel a the simulated effect of increasing the dose of ranibizumab from 0.5 mg (red curve) to 1 mg (dashed black curve) to 2 mg (green dot/dash curve) on the VEGF profiles of patient #40. For each doubling of the dose, the profiles shift to

the right by approximately 7.6 days (the ranibizumab $t_{1/2R}$ derived for this patient). In the Supporting Information (section S6), we show analytically that this is a general result of the model wherein each doubling of the antibody dose shifts the VEGF profiles to the right by approximately one $t_{1/2R}$. Thus, having an accurate estimate of $t_{1/2R}$ is important for accurately predicting the effect of dose on the duration of VEGF suppression.

Figure 7, panel b demonstrates the simulated effect in patient #40 of decreasing K_D by factors of 10 and 100 (from the *in vivo*

value of 21 000 pM) while keeping a fixed value of $t_{1/2R}$ (7.6 days). For each factor of 10 reduction in K_D , the VEGF profile shifts to the right by about 26 days. In the [Supporting Information](#) (section S6), we show analytically that each 10-fold decrease in K_D will in general shift the profile to the right by an amount equal to $t_{1/2R} \ln(10)/\ln(2)$, consistent with the simulated result for patient #40.

[Figure 7](#), panel c simulates the effect of increasing the MW of the VEGF binder from 48.35 kDa (ranibizumab) to 100 kDa, 200 kDa, and 500 kDa with a concomitant adjustment of the dose in proportion to MW. By reducing the elimination rate constants for R, VR, and RVR in accordance with the $MW^{-1/3}$ scaling law (eq 7), the curves shift to the right and rise more slowly.

In [Figure 7](#), panel d the effect of increasing MW at a constant dose of 0.5 mg is shown. At MWs of 200 and 500 kDa, the curves shift to the left at earlier times and crossover at later times. This complex behavior is also explained theoretically in the [Supporting Information](#) (section S6).

DISCUSSION

Our model provides new mechanistic insights into the intravitreal PK of large molecules such as ranibizumab and a reinterpretation of its PD effect on ocular VEGF levels in patients with wet AMD.

On the basis of simple geometric and biophysical concepts, we have shown that the $t_{1/2}$ values for large molecules should be proportional to their vitreous diffusion times (T_{diff}), with a proportionality factor determined by the fractional area of the vitreous/aqueous chamber interface where elimination is assumed to occur. Using Missel's anatomically accurate models of the eye for the rabbit, monkey, and human, we have estimated this fractional area (including the contribution from the space of Petit) and find it to be relatively constant. As a consequence, the proportionality factor between $t_{1/2}$ and T_{diff} should be approximately the same for all species with a value close to 4. We have verified this prediction by compiling data from PK studies in the rat, rabbit, monkey, and human with calculations of T_{diff} based on the Stokes–Einstein relation, in which the diffusivity was taken to be the same as in aqueous saline solution at 37 °C, and the hydrodynamic radius of the molecules assumed sphericity.

Use of the diffusion coefficients in physiological saline ([Table 1](#)) is consistent with Missel's work,¹⁹ which assumed that interactions between the diffusing species and the dilute collagen network of the vitreous would be negligible except for large polymeric molecules. In this regard, studies of hindered diffusion in aqueous collagen gels³² suggest a possible reduction in D by 10–40% for molecules with R_h values of 2–4 nm over the range of collagen concentrations seen in the vitreous humor (0.6–3 g/dL³³). On the basis of Perrin's equations, the effect of nonsphericity would increase R_h slightly (less than 20%) for molecules with axial ratios less than 4.³⁴ Together, these effects could conceivably increase T_{diff} by as much as two-fold from the calculated values in [Table 4](#). However, as noted in the derivation of eq 6, our expression for k_{el} is only an approximation for the mean passage time from the origin, which can be evaluated more precisely by considering the solution for the “first-passage problem”²³ at the center of the spherical geometry illustrated in [Figure 1](#). Preliminary calculations based on the latter, more formal treatment suggest that the proportionality factor between $t_{1/2}$ and T_{diff} in eq 6 is about 40% smaller than our estimate, and

this would largely compensate for the larger T_{diff} values. Such refinements to our IVT PK model will be a topic for future research.

It is important to note that the experimental $t_{1/2}$ values reported for ranibizumab in humans (7.2 and 8.6 days) are consistent with the theory and preclinical data from smaller preclinical animal species shown in [Figure 3](#). These values were derived from two independent clinical studies that used different methodologies, for example, aqueous humor sampling in a composite data set from patients with different retinal diseases by Krohne et al.¹¹ and a PK analysis of serum samples by Xu et al.¹² Our use of the mean value (7.9 days) and the variation around it, estimated from Xu's study, is central to the subsequent analysis of Saunders' VEGF data.

Using the RVR model of ranibizumab-VEGF binding, we provide an alternative analysis of Saunders' VEGF data in which the interplay between the assumed value of K_D and the estimated values of $t_{1/2}$ have been systematically explored over a wide range of K_D values ([Figure 5](#)). Because of the small variation observed in the quality of fit (see [Supporting Information](#), section S4), we conclude that the VEGF data alone are not sufficient to identify a unique value of K_D and distribution of $t_{1/2R}$ values. We have resolved this ambiguity by using the experimentally observed half-life for ranibizumab (7.9 days) to estimate the *in vivo* K_D value, which we find to be 21 326 pM (21.3 nM).

The large disparity between our *in vivo* estimate of K_D and the *in vitro* value used by Saunders of 46 pM (measured at 25 °C) could have a number of possible explanations. First, the *in vitro* determination of absolute K_D values is strongly platform dependent and may not reflect the true solution interaction of VEGF and anti-VEGF molecules,²⁰ whereas the relative binding constants for different anti-VEGF molecules under the same experimental conditions may be less sensitive. In this regard, studies of the binding of VEGF to the extracellular domain of the VEGF receptor using isothermal titration calorimetry, a solution-based thermodynamic method, gave K_D values of 12–38 nM at 20 °C.³⁵ Second, at body temperature (37 °C), K_D should be larger than at 25 °C, as the enthalpy of VEGF binding to polypeptides and large molecules is negative.^{35,36} Third, the *in vivo* K_D value could be influenced by other factors in the eye, for example, soluble VEGF receptors that could compete with anti-VEGF binders for VEGF molecules.³⁷ Finally, the Luminex assay used by Saunders to measure the aqueous humor levels of “free VEGF” may also be perturbed by endogenous or exogenous factors or subsequent steps in the sample preparation. Future experiments on the interaction of anti-VEGF binders and VEGF will be needed to resolve this disparity.

We believe it is important to have the correct $t_{1/2}$, K_D value and PK/PD model to accurately predict the dependence of the VEGF profiles on dose, K_D , and MW. As illustrated in [Figure 7](#) the ability to simulate the effects of these parameters on the VEGF profiles may help in the development of future therapies with a prolonged duration of VEGF suppression.

ASSOCIATED CONTENT

Supporting Information

The Supporting Information is available free of charge on the ACS Publications website at DOI: 10.1021/acs.molpharmaceut.5b00849.

Additional figures, formulas, data and analysis (PDF)

AUTHOR INFORMATION

Corresponding Authors

*E-mail: laurence.hutton-smith@pmb.ox.ac.uk.

*E-mail: norman.mazer@roche.com.

Author Contributions

The manuscript was written through contributions of all authors. All authors have given approval to the final version of the manuscript.

Notes

The authors declare the following competing financial interest(s): D.S. and N.A.M. are employees of F. Hoffmann-LaRoche Ltd. The remaining authors declare no competing financial interest.

ACKNOWLEDGMENTS

N.A.M. wishes to acknowledge Dr. Daniel Serafin for assistance using the plot digitizer and for helpful discussions related to this work. Funding provided to Wolfson Centre of Mathematical Biology by EPSRC and MRC (Grant No. EP/L016044/1). Additional funding provided by Roche Pharma Research and Early Development.

ABBREVIATIONS

Refer to Table 3 for Parameter Definition

D , diffusion coefficient; Fab, monoclonal antibody fragment; K_D , dissociation constant; IVT, intravitreal; $t_{1/2}$, half-life; MW , molecular weight; wet AMD, neovascular age-related macular degeneration; PK, pharmacokinetics; PD, pharmacodynamics; R_h , hydrodynamic radius; R, ranibizumab; RVR, ranibizumab-VEGF-ranibizumab complex; S and S^* , surface areas (see text for definitions); T_{diff} , vitreous diffusion time; VEGF or V , vascular endothelial growth factor; VR, VEGF-ranibizumab complex

REFERENCES

- (1) Bressler, N. M. Age-Related Macular Degeneration Is the Leading Cause of Blindness. *Arch Ophthalmol* **2004**, *291* (15), 1900–1901.
- (2) Rosenfeld, P. J.; Brown, D. M.; Heier, J. S.; Boyer, D. S.; Kaiser, P. K.; Chung, C. Y.; Kim, R. Y. Ranibizumab for Neovascular Age-Related Macular Degeneration. *N. Engl. J. Med.* **2006**, *355* (14), 1419–1431.
- (3) Penn, J. S.; Madan, A.; Caldwell, R. B.; Bartoli, M.; Caldwell, R. W.; Hartnett, M. E. Vascular Endothelial Growth Factor in Eye Disease. *Prog. Retinal Eye Res.* **2008**, *27* (4), 331–371.
- (4) Ferrara, N.; Damico, L.; Shams, N.; Lowman, H.; Kim, R. Development of Ranibizumab, an Anti-Vascular Endothelial Growth Factor Antigen Binding Fragment, as Therapy for Neovascular Age-Related Macular Degeneration. *Retina* **2006**, *26* (8), 859–870.
- (5) Meyer, C. H.; Krohne, T. U.; Holz, F. G. Concentrations of Unbound Bevacizumab in the Aqueous of Untreated Fellow Eyes after a Single Intravitreal Injection in Humans. *Acta Ophthalmol.* **2012**, *90* (1), 68–70.
- (6) Krohne, T. U.; Eter, N.; Holz, F. G.; Meyer, C. H. Intraocular Pharmacokinetics of Bevacizumab after a Single Intravitreal Injection in Humans. *Am. J. Ophthalmol.* **2008**, *146* (4), 508–512.
- (7) Mordenti, J.; Cuthbertson, R. A.; Ferrara, N.; Thomsen, K.; Berleau, L.; Licko, V.; Allen, P. C.; Valverde, C. R.; Meng, Y. G.; Fei, D. T. W.; Foure, K. M.; Ryan, A. M. Comparisons of the Intraocular Tissue Distribution, Pharmacokinetics, and Safety of 125 I-Labeled Full-Length and Fab Antibodies Following Intravitreal Administration. *Toxicol. Pathol.* **1999**, *27* (5), 536–544.
- (8) Gaudreault, J.; Fei, D.; Rusit, J.; Suboc, P.; Shiu, V. Preclinical Pharmacokinetics of Ranibizumab (rhuFabV2) after a Single Intra-

vitreal Administration. *Invest. Ophthalmol. Visual Sci.* **2005**, *46* (2), 726–733.

(9) Bakri, S. J.; Snyder, M. R.; Reid, J. M.; Pulido, J. S.; Ezzat, M. K.; Singh, R. J. Pharmacokinetics of Intravitreal Ranibizumab (Lucentis). *Ophthalmology* **2007**, *114* (12), 2179–2182.

(10) Bakri, S. J.; Snyder, M. R.; Reid, J. M.; Pulido, J. S.; Singh, R. J. Pharmacokinetics of Intravitreal Bevacizumab (Avastin). *Ophthalmology* **2007**, *114* (5), 855–859.

(11) Krohne, T. U.; Liu, Z.; Holz, F. G.; Meyer, C. H. Intraocular Pharmacokinetics of Ranibizumab Following a Single Intravitreal Injection in Humans. *Am. J. Ophthalmol.* **2012**, *154* (4), 682–686.

(12) Xu, L.; Lu, T.; Tuomi, L.; Jumbe, N.; Lu, J.; Eppler, S.; Kuebler, P.; Damico-Beyer, L. A.; Joshi, A. Pharmacokinetics of Ranibizumab in Patients with Neovascular Age-Related Macular Degeneration: A Population Approach. *Invest. Ophthalmol. Visual Sci.* **2013**, *54* (3), 1616–1624.

(13) Gadkar, K.; Pastuskovas, C. V.; Le Couter, J. E.; Elliott, J. M.; Zhang, J.; Lee, C. V.; Sanowar, S.; Fuh, G.; Kim, H. S.; Lombana, T. N.; Spiess, C.; Nakamura, M.; Hass, P.; Shatz, W.; Meng, Y. G.; Scheer, J. M. Design and Pharmacokinetic Characterization of Novel Antibody Formats for Ocular Therapeutics. *Invest. Ophthalmol. Visual Sci.* **2015**, *56* (9), 5390–5400.

(14) Chuang, L.-H.; Wu, W.-C.; Yeung, L.; Wang, N.-K.; Hwang, Y.-S.; Chen, K.-J.; Kuo, J. Z.-C.; Lai, C.-C. Serum Concentration of Bevacizumab after Intravitreal Injection in Experimental Branch Retinal Vein Occlusion. *Ophthalmic Res.* **2011**, *45* (1), 31–35.

(15) Muether, P. S.; Hermann, M. M.; Viebahn, U.; Kirchof, B.; Fauser, S. Vascular Endothelial Growth Factor in Patients with Exudative Age-Related Macular Degeneration Treated with Ranibizumab. *Ophthalmology* **2012**, *119* (10), 2082–2086.

(16) Muether, P. S.; Hermann, M. M.; Dröge, K.; Kirchof, B.; Fauser, S. Long-Term Stability of Vascular Endothelial Growth Factor Suppression Time under Ranibizumab Treatment in Age-Related Macular Degeneration. *Am. J. Ophthalmol.* **2013**, *156* (5), 989.

(17) Saunders, D. J.; Muether, P. S.; Fauser, S. A Model of the Ocular Pharmacokinetics Involved in the Therapy of Neovascular Age-Related Macular Degeneration with Ranibizumab. *Br. J. Ophthalmol.* **2015**, *99*, 1554–1559.

(18) Papadopoulos, N.; Martin, J.; Ruan, Q.; Rafique, A.; Rosconi, M. P.; Shi, E.; Pyles, E. a.; Yancopoulos, G. D.; Stahl, N.; Wiegand, S. J. Binding and Neutralization of Vascular Endothelial Growth Factor (VEGF) and Related Ligands by VEGF Trap, Ranibizumab and Bevacizumab. *Angiogenesis* **2012**, *15* (2), 171–185.

(19) Missel, P. J. Simulating Intravitreal Injections in Anatomically Accurate Models for Rabbit, Monkey, and Human Eyes. *Pharm. Res.* **2012**, *29* (12), 3251–3272.

(20) Yang, J.; Wang, X.; Fuh, G.; Yu, L.; Wakshull, E.; Khosravi, M.; Day, E. S.; Demeule, B.; Liu, J.; Shire, S. J.; Ferrara, N.; Yadav, S. Comparison of Binding Characteristics and In Vitro Activities of Three Inhibitors of Vascular Endothelial Growth Factor A. *Mol. Pharmaceutics* **2014**, *11*, 3421–3430.

(21) Harpaz, Y.; Gerstein, M.; Chothia, C. Volume Changes on Protein Folding. *Structure* **1994**, *2* (7), 641–649.

(22) Park, J.; Bungay, P. M.; Lutz, R. J.; Augsburger, J. J.; Millard, R. W.; Sinha Roy, A.; Banerjee, R. K. Evaluation of Coupled Convective-Diffusive Transport of Drugs Administered by Intravitreal Injection and Controlled Release Implant. *J. Controlled Release* **2005**, *105* (3), 279–295.

(23) Bressloff, P. C.; Newby, J. M. Stochastic Models of Intracellular Transport. *Rev. Mod. Phys.* **2013**, *85* (1), 135–196.

(24) Meyer, C. H.; Krohne, T. U.; Holz, F. G. Intraocular Pharmacokinetics After a Single Intravitreal Injection Of 1.5 Mg Versus 3.0 Mg Of Bevacizumab In Humans. *Retina* **2011**, *31* (9), 1877–1884.

(25) Ferrara, N. Vascular Endothelial Growth Factor and Age-Related Macular Degeneration: From Basic Science to Therapy. *Nat. Med.* **2010**, *16* (10), 1107–1111.

(26) Zhu, Q.; Ziemssen, F.; Henke-fahle, S.; Tatar, O.; Szurman, P.; Aisenbrey, S.; Schneiderhan-marra, N.; Xu, X.; Grisanti, S. Vitreous

Levels of Bevacizumab and Vascular Endothelial Growth Factor-A in Patients with Choroidal Neovascularization. *Ophthalmology* **2008**, *115*, 1750–1756.

(27) The MathWorks Inc. *MATLAB User Guide R2015b: Global Optimization Toolbox*, 2015.

(28) Tasman, W.; Jaeger, E. A. *Duane's Ophthalmology 2013*; Lippincott Williams & Wilkins, 2013.

(29) Fontana, S. T.; Brubaker, R. F. Volume and Depth of the Anterior Chamber in the Normal Aging Human Eye. *Arch. Ophthalmol.* **1980**, *98*, 1803–1808.

(30) Toris, C. B.; Yablonski, M. E.; Wang, Y. L.; Camras, C. B. Aqueous Humor Dynamics in the Aging Human Eye. *Am. J. Ophthalmol.* **1999**, *127* (4), 407–412.

(31) Sha, O.; Kwong, W. H. Postnatal Developmental Changes of Vitreous and Lens Volumes in Sprague-Dawley Rats. *Neuroembryol. Aging* **2006**, *4* (4), 183–188.

(32) Ramanujan, S.; Pluen, A.; McKee, T. D.; Brown, E. B.; Boucher, Y.; Jain, R. K. Diffusion and Convection in Collagen Gels: Implications for Transport in the Tumor Interstitium. *Biophys. J.* **2002**, *83* (3), 1650–1660.

(33) Bishop, P. N. Structural Macromolecules and Supramolecular Organisation of the Vitreous Gel. *Prog. Retinal Eye Res.* **2000**, *19* (3), 323–344.

(34) Macchioni, A.; Ciancaleoni, G.; Zuccaccia, C.; Zuccaccia, D. Determining Accurate Molecular Sizes in Solution through NMR Diffusion Spectroscopy. *Chem. Soc. Rev.* **2008**, *37* (3), 479–489.

(35) Stutfeld, E. *Structural and Functional Characterization of the Extracellular Domain of Vascular Endothelial Growth Factor Receptors: Their Role in Receptor Activation and Use as Therapeutic Targets*. Doctoral Dissertation, University of Basel, Basel, Switzerland, 2012.

(36) Reille-Seroussi, M.; Gaucher, J.-F.; Desole, C.; Gagey-Eilstein, N.; Brachet, F.; Broutin, I.; Vidal, M.; Broussy, S. Vascular Endothelial Growth Factor Peptide Ligands Explored by Competition Assay and Isothermal Titration Calorimetry. *Biochemistry* **2015**, *54* (33), 5147–5156.

(37) Davuluri, G.; Espina, V.; Petricoin, E. F.; Ross, M.; Deng, J.; Liotta, L. A.; Glaser, B. M. Activated VEGF Receptor Shed Into the Vitreous in Eyes With Wet AMD. *Arch. Ophthalmol.* **2009**, *127* (5), 613–621.